

Article

Biochar Nanoparticles over TiO₂ Nanotube Arrays: A Green Co-Catalyst to Boost the Photocatalytic Degradation of Organic Pollutants

Marco Pinna ¹, Gilberto Binda ¹, Marco Altomare ², Marcello Marelli ³, Carlo Dossi ⁴,
Damiano Monticelli ¹, Davide Spanu ^{1,*} and Sandro Recchia ^{1,*}

- ¹ Department of Science and High Technology, University of Insubria, Via Valleggio 11, 22100 Como, Italy; mpinna@uninsubria.it (M.P.); gilberto.binda@uninsubria.it (G.B.); damiano.monticelli@uninsubria.it (D.M.)
² Photo-Catalytic Synthesis Group, MESA+ Institute for Nanotechnology, University of Twente, P.O. Box 217, 7500 AE Enschede, The Netherlands; m.altomare@utwente.nl
³ National Research Council of Italy (CNR), Istituto SCITEC, Via C. Golgi 19, 20133 Milan, Italy; marcello.marelli@scitec.cnr.it
⁴ Department of Theoretical and Applied Sciences, University of Insubria, Via Dunant, 3, 22100 Varese, Italy; carlo.dossi@uninsubria.it
* Correspondence: d.spanu1@uninsubria.it (D.S.); sandro.recchia@uninsubria.it (S.R.); Tel.: +39-0312386451 (D.S.); +39-0312386450 (S.R.)

Abstract: Biochar nanoparticles (BC NPs), produced by low temperature pyrolysis (350 °C) of microalgae (*Nannochloropsis* sp.) and nutshells, are proposed as low-cost and sustainable co-catalysts to promote the photocatalytic activity of TiO₂ nanotube (NT) arrays towards the degradation of methylene blue (MB) used as an organic pollutant model molecule. BC NPs (size < 25 nm) were obtained by treating bulk BC (i.e., biomass after pyrolysis) by sonication–centrifugation cycles in a water solution. The filtered BC NPs dispersion was deposited by simple drop-casting on the TiO₂ NT support. The BC loading was varied by performing multiple depositions. Photocatalytic experiments under UV light (365 nm) revealed that the decoration with BC NPs significantly improves the TiO₂ photoactivity. Such enhancement is mainly influenced by the amount of BC deposited; upon optimizing the BC deposition conditions, the rate of photocatalytic degradation of MB increases approximately three times with respect to bare TiO₂, almost irrespective of the nature of the raw material. The greater photocatalytic activity of BC-TiO₂ can be attributed to the synergistic combination of reactant/product adsorption and catalytic degradation of the adsorbed organic pollutant, as well as an improved charge carrier separation and electron transfer.

Keywords: biochar; biomass; TiO₂ nanotubes; photocatalysis; methylene blue; microalgae; nutshell; carbon dots; organic pollutant; environmental remediation



Citation: Pinna, M.; Binda, G.; Altomare, M.; Marelli, M.; Dossi, C.; Monticelli, D.; Spanu, D.; Recchia, S. Biochar Nanoparticles over TiO₂ Nanotube Arrays: A Green Co-Catalyst to Boost the Photocatalytic Degradation of Organic Pollutants. *Catalysts* **2021**, *11*, 1048. <https://doi.org/10.3390/catal11091048>

Academic Editor: Lucian Baia

Received: 5 August 2021

Accepted: 29 August 2021

Published: 29 August 2021

Publisher's Note: MDPI stays neutral with regard to jurisdictional claims in published maps and institutional affiliations.



Copyright: © 2021 by the authors. Licensee MDPI, Basel, Switzerland. This article is an open access article distributed under the terms and conditions of the Creative Commons Attribution (CC BY) license (<https://creativecommons.org/licenses/by/4.0/>).

1. Introduction

With the accelerated expansion of worldwide industrialization and urbanization, environmental pollution is increasingly becoming a serious global issue faced by humankind [1]. Therefore, green, cost-effective, and efficient ways to resolve this adverse situation have been extensively studied by researchers in recent decades. Among the various strategies conceived to solve this global problem, heterogeneous photocatalysis, in which the naturally available and clean energy of the sun can be exploited by semiconductors (e.g., TiO₂, α-Fe₂O₃, ZnO), has emerged as one of the most promising technologies, especially for water purification [2,3]. Photocatalytic materials have been widely studied for the degradation and removal of many inorganic [4–6] and organic [7,8] pollutants in natural and waste waters.

Although a broad variety of semiconductors have been explored so far, titanium dioxide (TiO₂) is still the most studied material, owing to its non-toxicity, stability against

(photo)corrosion, and low cost [9]. Nanostructured TiO₂ (e.g., nanoparticles, nanotubes, nanorods) is extensively employed as it can provide a larger surface area and more efficient charge collection (transfer) by redox species in the reaction environment compared to bulk TiO₂ [10]. In addition, co-catalysts forming heterojunctions on TiO₂ are also employed to further promote charge separation and transfer [11–13] or to enhance the catalytic activity (e.g., providing new reaction sites and pathways or increasing reactant adsorption) [6,13,14]; metal oxides (e.g., WO₃, Fe₂O₃) [15–17], metals (e.g., Au, Pt) [11,18], or metal alloys [19,20] are typically used for this purpose. Carbon-based materials (e.g., carbon nanotubes [21,22], graphene oxide [23], and carbon dots [24,25]) have also been proposed as alternative co-catalysts or supports for TiO₂-based photocatalysts.

In this context, biochar (BC), a porous carbonaceous material produced from biomass feedstocks via pyrolysis, has recently been proposed as a greener supporting carbon material for powdered photocatalytic platforms [26–28] and, in a fewer reports, as co-catalytic nanoparticles supported on nanostructured TiO₂ [29]. As one main advantage, the employment of BC allows for strongly reducing the environmental footprint and costs associated with the photocatalyst synthesis compared to traditional noble metal- and carbon-based materials; its production is highly sustainable, as waste biomasses can be used as raw materials [30,31]. Many other advantages of using biochar are reported in the literature concerning the implementation of renewable energies as easy metal recovery [32] and its application in fuel cells [33]. The unique physicochemical properties of BC make it an ideal candidate for (photo)catalytic applications due to its high specific surface area, easily tunable functional groups, chemical stability, and electrical conductivity [27,34,35]. The coupling of BC with TiO₂ can therefore offer a synergistic combination of reactant/product adsorption and catalytic degradation of the adsorbed pollutants, as well as an improved charge carrier separation and electron transfer system, which result in a significantly enhanced overall photocatalytic efficiency [27,36].

The properties of BC can be tuned by changing pyrolysis temperature and biomass feedstocks [37–39] in order to reach the best (photo)catalytic performances. Highly conductive, graphitized BC produced at high temperatures (800–1000 °C), characterized by a high specific surface area and porosity, is often preferred for catalytic applications, as BC is commonly employed as a support for photocatalyst nanoparticles [27,40]. Activating agents (e.g., KOH, H₃PO₄) are also employed to further promote the creation of pores and to enable the formation of surface functional groups, which are partially lost at high temperatures due to the graphitization of the material [41]. At temperatures above 500–600 °C, in fact, the degradation of organic matter with stronger chemical bonds occurs, leading to a loss of functionalization. Despite their high performances, the required harsh pyrolysis conditions drastically reduce (i) the environmental friendliness of BC fabrication, (ii) BC yield [37], and (iii) the natural self-doping of BC (which strictly depends on the feedstock chemical composition and pyrolysis temperature) [42]. In contrast, the employment of milder conditions, e.g., chemical-free slow pyrolysis at low temperatures (<400 °C), can provide a solution to these limitations leading to high production yields of naturally functionalized and self-doped BC with improved adsorptive properties [43–46]. Considering that functionalized materials are highly sought in (photo)catalytic applications, the combination of low temperature pyrolysis with heteroatom-rich biomass feedstocks, e.g., microalgae, should be beneficial, as highly functionalized biochar with improved adsorption properties is produced. However, the limited specific surface area of BC produced at low temperature hinders its typical employment as supporting material for powdered photocatalysts, and that is why it is more rarely studied. Downsizing of BC to quasi-spherical nanoparticles, e.g., by forming carbon dots by sonication, centrifugation, and filtration [47]), may instead open the possibility to exploit such highly functionalized BC nanoparticles as co-catalytic material deposited onto nanostructured photocatalytic layers; the BC downsizing process results in a greatly increased specific surface area and enhanced electronic and optical properties [47,48]. Moreover, the production of BC NPs should be not considered less green than bulk materials, as the employment of chemicals or harsh conditions (that may hinder

the sustainability of the production process) is not involved. In this light, BC NPs can be deemed as a green co-catalyst that can enable the possibility to fabricate a supported photocatalytic layer rather than conventional powdered photocatalytic platforms produced by using bulk biochar.

In light of these considerations, BC nanoparticles produced by the slow pyrolysis at a low temperature (350 °C) of microalgae (*Nannochloropsis* sp.) and nutshell were used in this work as a co-catalyst on the surface of anodic TiO₂ nanotube arrays (TiO₂ NTs) to boost the photocatalytic activity towards the degradation of methylene blue, selected as an organic pollutant model. These biomass feedstocks were selected because of their markedly different composition, with microalgae-derived BC being noticeably more polar than the nutshell-derived one. The investigation of these diverse materials aims at evaluating the effect of the nature of the starting biomass feedstock on the promotion of the catalytic performances. The influence of other parameters such as BC loading and photocatalytic conditions were evaluated, too.

2. Results and Discussion

2.1. Bulk BC Characterization

Microalgae- and nutshell-derived biochar used for the fabrication of BC-TiO₂ photocatalysts were produced and fully characterized in a previous work [46]. Briefly, BC having high surface rugosity (see SEM images in Figure S1) was produced with quite high yield by using both lignocellulosic and microalgae feedstocks (34 ± 2% and 41 ± 4% yields, respectively). Concerning the elemental composition of these materials, heteroatom content (P and N) of MBC is tenfold of that observed for NBC (Figure S2): this evidence is coherent with the higher amount of protein and lipids in microalgae. Furthermore, a more marked presence of aromatic C–H, as well as of –OH, C=O, C–O–C, and N–H functional groups, was found in MBC compared to NBC, in which no carbonyl bands were detected. Such features can be ascribed to the diverse nature of the feedstocks and to the catalytic effect of alkali (Na and K) and alkaline earth (Mg and Ca) metals during pyrolysis (see Figure S2 for alkali and alkaline earth contents); these chemicals, massively present in microalgae, can promote the formation of light oxygenates via ring fragmentation reactions of carbohydrates [46]. Finally, XRD analysis showed that no crystalline phases were formed during pyrolysis, most likely due to the low temperature of the thermal treatment [41].

2.2. Characterization of TiO₂ and BC-TiO₂ Photocatalysts

After pyrolysis, bulk BC powder was dispersed in ultrapure water (10 g/L) and sonicated for 1 h to induce the partial breaking of BC to nanosized particles. Then, the so obtained BC suspension was centrifuged, and the supernatant was filtered (0.2 µm pore size membrane) and collected. A schematic representation of the BC NPs fabrication route is depicted in Figure 1.

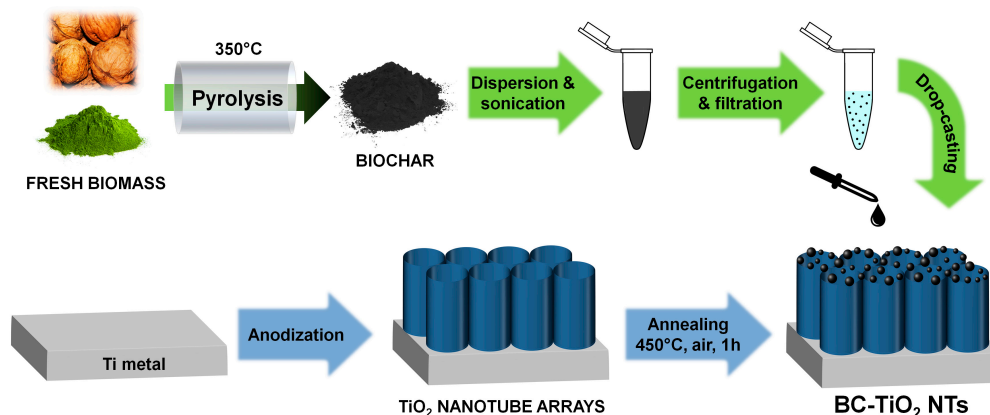


Figure 1. Schematic representation of the steps involved in the fabrication of BC-TiO₂ photocatalysts.

As shown in Figure 2, BC NPs having an average size of ~ 2 nm are present in the filtered aqueous solution. This suspension was drop-casted onto the TiO₂ support (Figure 1) with the aim of forming composite BC NPs-TiO₂ materials.

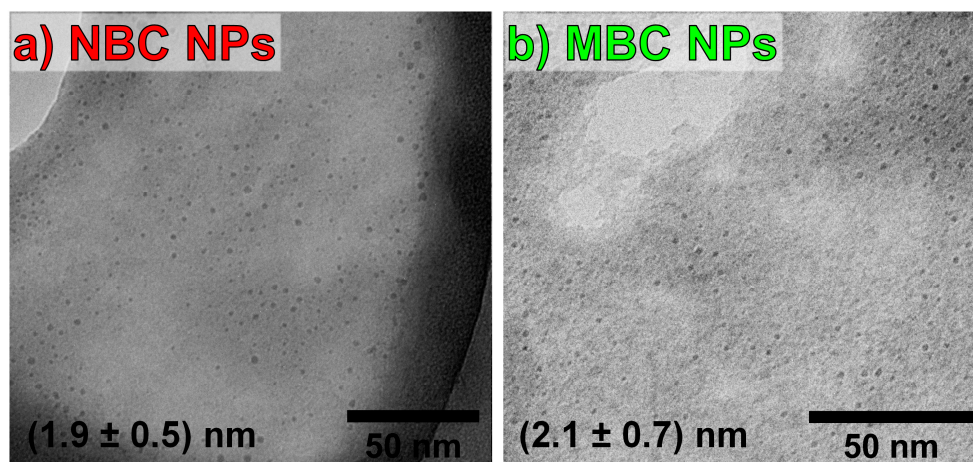


Figure 2. TEM images of (a) NBC and (b) MBC NPs produced by performing the procedure depicted in Figure 1 and described in the Materials and Methods section.

Cross-section and top-view SEM images of TiO₂ nanotube arrays used in this work are shown in Figure 3. The morphology of tubes appears well-ordered: an inner diameter of 104 ± 10 nm and a length of 5.6 ± 0.5 μ m were measured over the entire surface of the photocatalyst. Such length, easily tunable by adjusting the anodization time, was selected as it proved to be a good compromise between high light harvesting and limited charge carrier recombination [49].

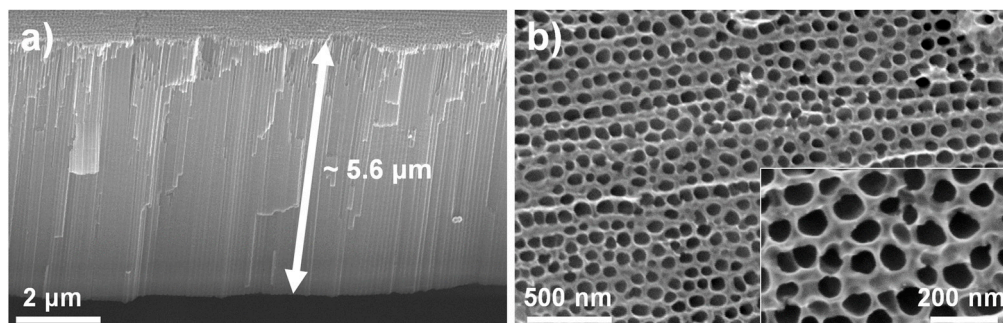


Figure 3. SEM images of (a) cross-section and (b) top-view of bare TiO₂ nanotubes (inset: magnified top-view image).

These one-dimensional TiO₂ nanostructures were decorated with MBC or NBC nanoparticles produced by multiple sonication–centrifugation steps, as described in the Materials and Methods section. As shown in Figure 4a,e, BC nanoparticles (diameter < 25 nm) are present at the surface of the TiO₂ nanotubes, already after a single drop-casting deposition (samples 1-MBC-TiO₂ and 1-NBC-TiO₂). This evidence suggests the suitability of the employed strategy for the production and deposition of BC nanoparticles.

As can be observed in Figure 4, the number and density of carbonaceous nanoparticles on the surface of the NTs arrays increase along with the number of depositions. This is particularly clear for the NBC-TiO₂ samples (see Figure 4e–h), while for the MBC-TiO₂ ones (Figure 4a–d) the effect is less visible; NBC-decorated NTs appear to be more heavily loaded with co-catalyst when compared to MBC-decorated ones. This evidence would indicate that both the number of drop-casting depositions and the nature of the feedstock heavily impact the BC loading on the photocatalysts.

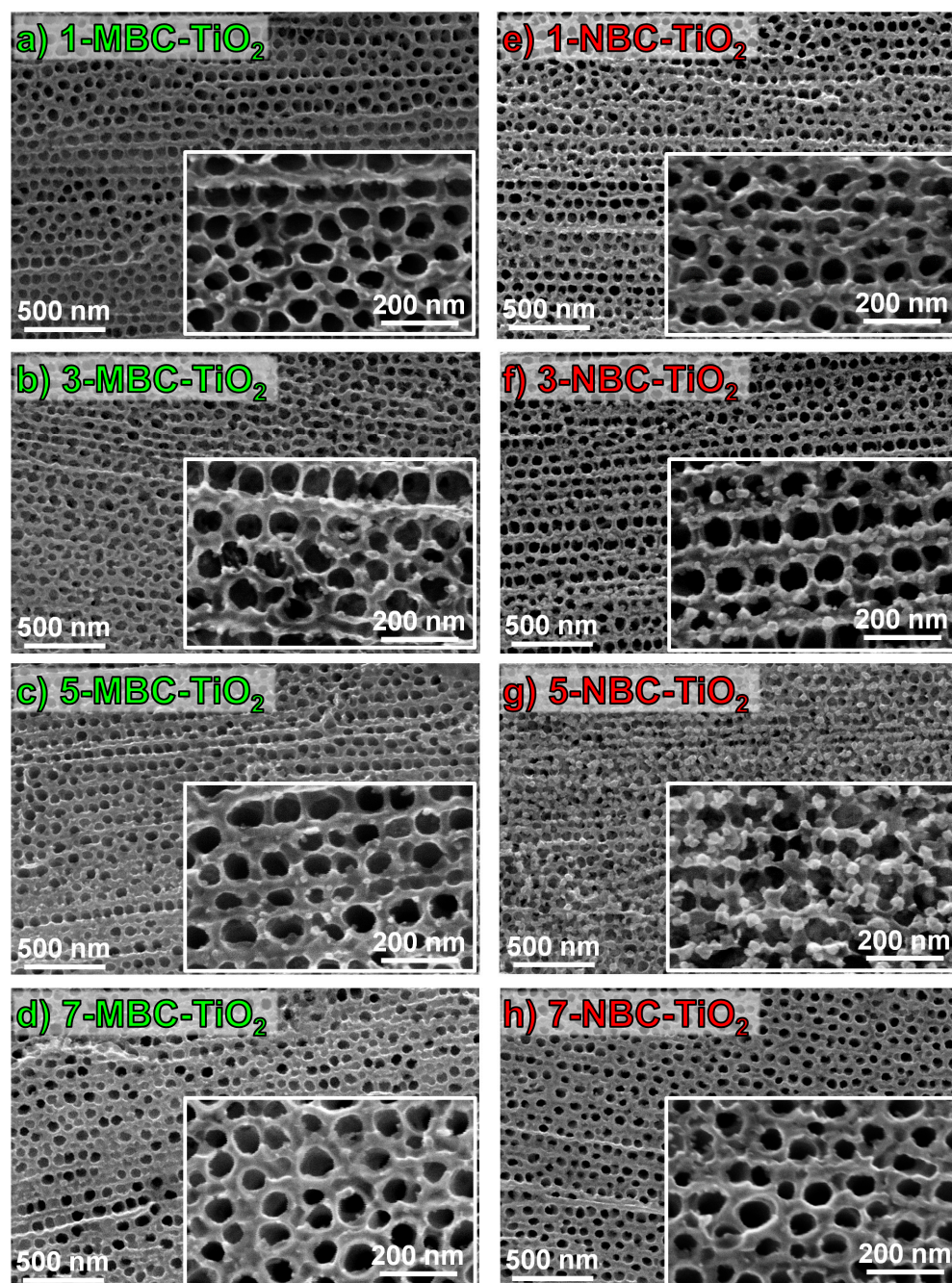


Figure 4. SEM top-view images of the samples obtained by depositing microalgae- (a–d) and nutshell-derived (e–h) BC NPs on the surface of TiO₂ nanotube arrays. Different BC loadings were achieved by performing multiple drop-casting depositions: samples after (a,e) 1, (b,f) 3, (c,g) 5, and (d,h) 7 depositions are depicted. Insets: magnified SEM top-view images.

No significant difference of the nanoparticle morphology was observed as a function of the number of depositions (see size distributions in Figure 5), since the shape of the BC co-catalysts remained nearly spherical. Only the nature of the feedstock seems to influence the BC NPs' morphology; as depicted in Figure 5, NBC NPs are larger and exhibit a wider dimensional distribution (24.2 ± 7.8 nm) with respect to MBC ones (15.3 ± 4.0 nm). Such NP size indicates the occurrence of an agglomeration process during drop-casting deposition, as NPs suspended in the aqueous solution have a much lower dimension (~ 2 nm, see Figure 2). The difference between NBC and MBC NPs in terms of agglomeration degree can be ascribed to the diverse hydrophilicity of the materials. In detail, NBC is

more hydrophobic than MBC, most likely due to the absence of a polar surface functional group [46]; according to the literature, the more hydrophobic BC NPs are, the higher their tendency to agglomerate in clusters is [50]. Such a consideration is also well in line with the much higher BC loading observed in NBC-TiO₂ materials. As a confirmation of the occurrence of the agglomeration process, only a few distinct NPs are discernable when carrying out the seven drop-casting depositions (7-MBC-TiO₂ and 7-NBC-TiO₂); most of the deposited carbonaceous material clustered in a homogeneous thin film covering the surface of the TiO₂ nanotubes (see Figure 4d,h).

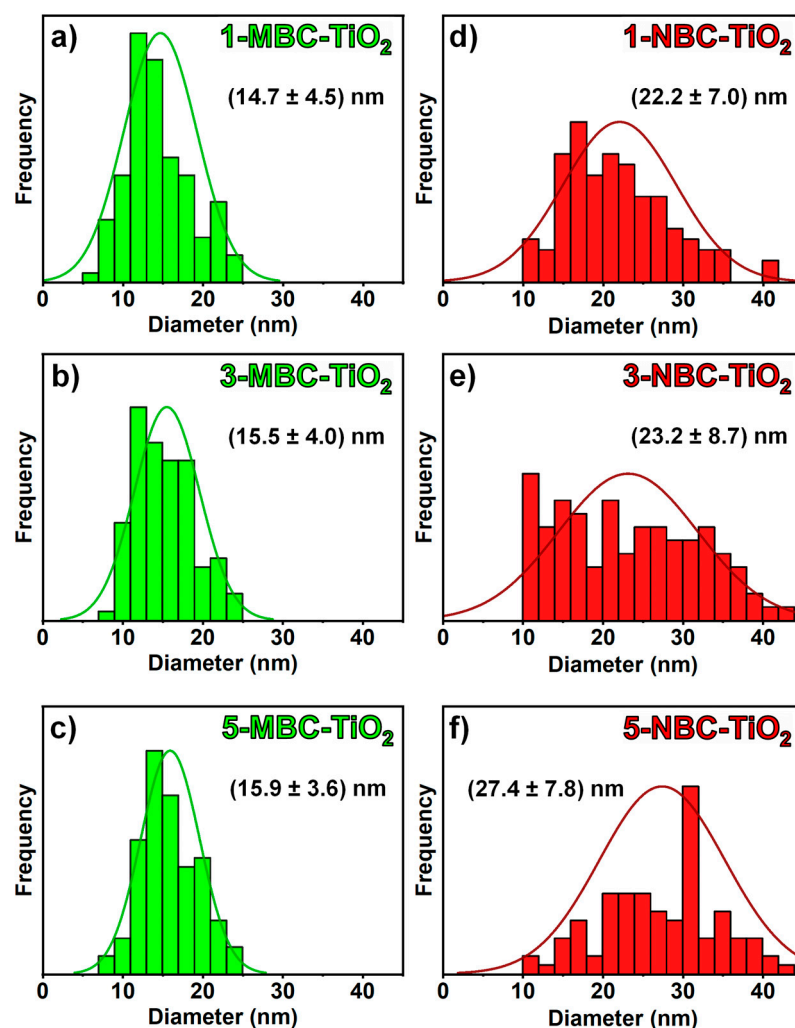


Figure 5. Size distributions of BC NPs in samples after (a,d) 1, (b,e) 3, (c,f) and 5 depositions. 7-NBC-TiO₂ and 7-MBC-TiO₂ samples were not considered in this morphological evaluation owing to the impossibility of identifying well-defined NPs due to the formation of agglomerated carbonaceous film. Refer to Figure 4 for SEM images of these samples.

Besides the investigation of compositional and morphological features of BC-TiO₂ materials, XRD analysis (reported in Figures 6 and S3) was performed to determine if the thermal treatment resulted in the crystallization of the amorphous TiO₂ and which phases were formed. Diffraction peaks at 25.3°, 48°, 52.7°, and 59.2° were observed for the annealed sample: these peaks are attributed to the (101), (200), (105), and (211) planes of anatase TiO₂. Additional peaks were observed for both the treated (annealed) and untreated samples at 38.3°, 38.8°, 40°, 52.8°, 70.5°, 76.6°, and 78°. These peaks can be attributed to the (002), (100), (101), (102), (110), (103), and (112) planes of hexagonal titanium, i.e., they can be associated with the metallic Ti support. Rutile formation was not observed, as, according to the literature, it would take place through nucleation at the oxide/metal substrate interface

upon prolonged thermal treatments or at higher temperatures [51,52]. As expected, XRD performed on BC-decorated samples (Figure 6, green and red lines) showed that no TiO_2 phase modifications are induced by the deposition of biochar. Moreover, no peaks that could be ascribed to the presence of crystalline carbon phases are visible, likely owing to the low amount and amorphous nature of the synthesized biochar.

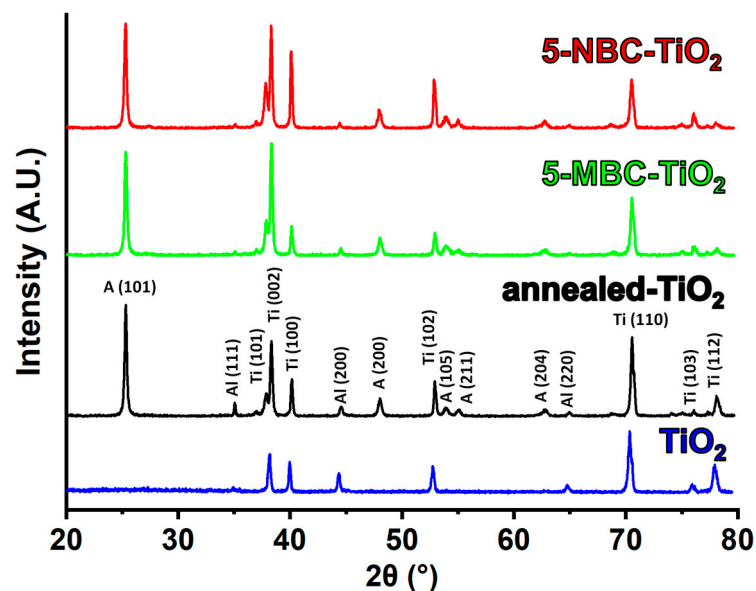


Figure 6. XRD pattern of as-formed (blue line) and crystalline TiO_2 nanotubes (black line), 5-MBC- TiO_2 (green line), and 5-NBC- TiO_2 (red line). The peak labels are indicated as follows: A = Anatase, Ti = Titanium (substrate), Al = Aluminum (sample holder).

Diffusive reflectance UV-vis spectra were also recorded for all the samples (Figures 7 and S4) to investigate the potential effect of BC NPs in inducing a redshift in the light absorption spectrum from UV to the visible region: this feature is sometimes reported for bulk BC when used as supporting material for powdered TiO_2 photocatalysts [36]. As expected, all the samples show high absorbance values for wavelengths lower than 380 nm, in line with the anatase TiO_2 composition of the NTs. Moreover, periodic absorption signals are always present even in the undecorated TiO_2 sample: this spectroscopic effect is most likely due to scattering inside the nanotube array [53] as already reported in previous works [54,55]. Interesting differences were found when decorating TiO_2 with BC NPs. In detail, 5-NBC- TiO_2 presents a broad and weak absorption peak in the 400–600 nm range, not present in any other sample, and the 5-MBC- TiO_2 sample presents a peculiar peak with a relative maximum absorbance at 331 nm. The presence of this peak can be ascribed to the π - π^* absorption typical of the aromatic system [56]; this assignment is also strengthened by the evidence of aromatic absorptions in the ATR spectrum recorded on such material [46]. Regarding the broad and weak absorption band present in the nutshell-derived sample, an analogous relatively weak absorbance in the visible region is widely reported in the literature [28,36,57,58], and this signal is generally attributed to the biochar content and to the interaction of the TiO_2 with BC (Ti-O-C bonds). The low intensity of this absorption signal is reasonably ascribed to the low BC loading on the photocatalyst. Despite these differences in the UV absorption spectra, the energy band gaps (E_g), estimated using the Kubelka–Munk method (see inset in Figure 6) for TiO_2 and BC- TiO_2 materials, show no significant differences, ruling out the occurrence of shifts in the E_g , which remains in the UV light region even after decoration with BC NPs ($E_g \sim 3.3$ eV for all the samples).

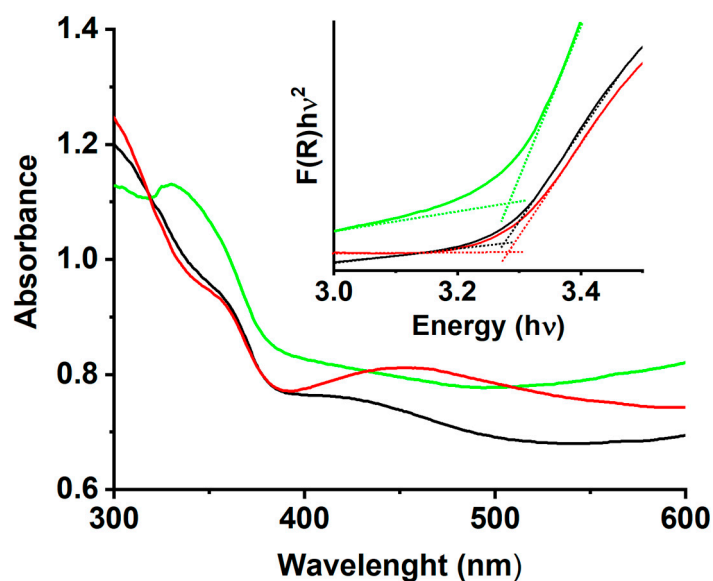


Figure 7. DR-UV spectra of bare TiO₂ nanotubes (black line), 5-NBC-TiO₂ (red line), and 5-MBC-TiO₂ (green line). Inset: Kubelka–Munk plots for the samples.

2.3. Assessment of the Photocatalytic Performances

Prior to proceeding with photocatalytic experiments, MB stability under UV irradiation was preliminary carried out. A 10 mg/L dye solution was stirred and irradiated by UV light in the absence of any photocatalyst; as a result, no decrease of MB concentration was observed after three hours, demonstrating that MB does not undergo decomposition under these experimental conditions. Then, the presence of no light-assisted adsorption/degradation processes at the photocatalyst surface was investigated; tests were carried out by stirring the MB solution under dark conditions in the presence of bare TiO₂ and BC-TiO₂ photocatalysts. Even in these cases, no appreciable decreases of MB concentrations were observed for all tested catalysts after three hours using the bare or five times decorated materials (TiO₂, 5-NBC-TiO₂ and 5-MBC-TiO₂). The absence of remarkable absorption phenomena can be ascribed to the low amount of BC deposited on the TiO₂ nanotubes.

The photocatalytic tests were then performed to assess the effects of the BC NPs' loading on the photocatalytic performances. It should be underlined that mild photocatalytic conditions were intentionally used to enhance differences between each system and to better analyze the kinetic of MB degradation; experiments under boosted conditions are discussed later.

A kinetic study over short-term experiments (three hours) was preliminary carried out. As shown in Figure 8, the presence of BC NPs significantly enhances the photocatalytic activity towards the degradation of MB, whatever their origin and amount. This evidence clearly demonstrates the suitability of using microalgae- and nutshell-derived BC NPs as co-catalysts.

Significant differences in photocatalytic efficiency were found by varying both the nature of the biomass feedstock and the loading of BC NPs on TiO₂ nanotubes. For both systems, the degradation rate raises with the amount of co-catalyst (i.e., with the number of drop-casting depositions), reaching a maximum after five depositions (see Figure 8a,b); compared to undecorated TiO₂, 2.5- and 2.8-times larger amounts of MB were removed after three hours by 5-MBC-TiO₂ and 5-NBC-TiO₂, respectively. When loading more carbonaceous material, i.e., by performing the drop-casting procedure seven times, a decrease in photocatalytic efficiency was observed (see samples 7-MBC-TiO₂ and 7-NBC-TiO₂ in Figure 8). These experimental findings are well in line with the typical bell-shaped behavior reported for the photocatalytic efficiency when varying the loading of co-catalysts [14].

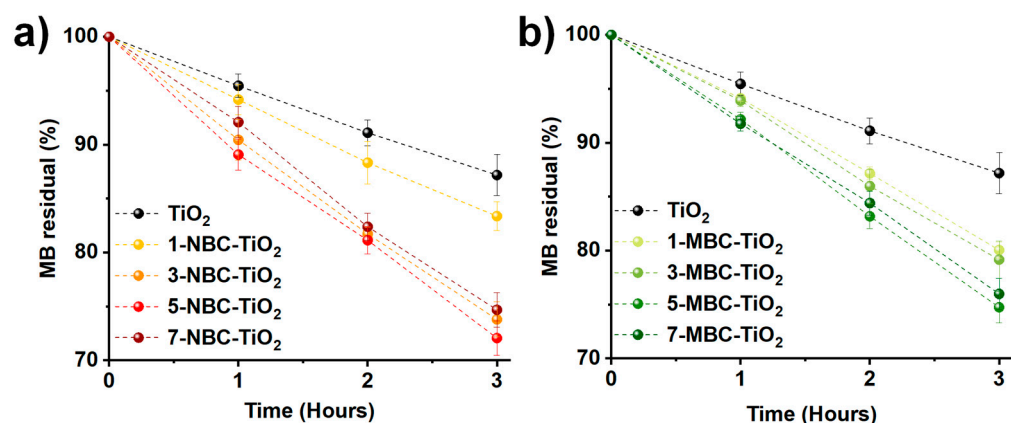


Figure 8. Effect of BC loading on the degradation of MB by nutshell—(a) and microalgae—(b) derived photocatalysts.

Concerning the reaction pathway, since it was impossible to observe MB degradation via adsorption mechanism (i.e., in the absence of light irradiation) or photodecomposition of MB itself (i.e., in the absence of the photocatalyst), it appears clear that the MB degradation mechanism involves a photocatalytic process on the surface of BC-TiO₂ materials. It is widely accepted that the overall process involves the formation of superoxide radicals, generated by a reaction with holes at the semiconductor surface, which quickly react with the dye molecules, breaking them down into smaller molecular fragments and eventually to CO₂ and water [36]. This process is greatly enhanced by the sorption of MB on the BC NPs' surfaces. Additionally, as metal particles (e.g., Pt) do when decorated on a semiconductor surface, biochar can shuttle and trap electrons [27]; this results in an improvement of charge carrier separation in the semiconductor, thus reducing the charge carrier recombination rate [28]. Based on the information present in literature, it can be reasonably supposed that the photocatalytic process occurring at the surface of the prepared materials is the combination of an adsorption process on BC nanoparticles and an oxidation reaction happening due to the presence of holes on the surface of the TiO₂ nanotubes array. In this light, it is reasonable to suggest that the decomposition process is enhanced for samples which show isolated BC nanoparticles, while the formation of a BC film might lead to a decrease in photocatalytic activity due to a reduction of TiO₂ surface available for the oxidation process. This interpretation explains the lower photocatalytic activity of 7-BC-TiO₂ samples compared to that of 5-BC-TiO₂ ones; in the former, a dense carbonaceous film completely covers the surface of TiO₂ (where the oxidation of MB most likely takes place), whereas the latter shows well-defined BC nanoparticles and a more available TiO₂ surface.

Based on these results, the most active materials, i.e., 5-NBC-TiO₂ and 5-MBC-TiO₂, were studied in view of their photocatalytic activity during longer experiments (up to 51 h) to assess their (photo) stability and gain insights into the degradation kinetics. MB degradation profiles are shown in Figure 9.

As can be observed for the long kinetics experiments, the MBC-decorated TiO₂ is the most efficient photocatalyst for the degradation of MB, doubling the reaction rate compared to bare TiO₂ (see Figure 10) and completely mineralizing the dye within 48 h. In contrast, undecorated and nutshell-derived materials were unable to completely degrade the azo dye and exhibited a less efficient behavior, even though 5-NBC-TiO₂ performs even better than 5-MBC-TiO₂ within the first 3 h (see Figures 8 and 10). This behavior might be ascribed to a poisoning effect induced by methylene blue which is more marked for TiO₂ and 5-NBC-TiO₂ rather than for 5-MBC-TiO₂. A second 3-h MB degradation was then performed on the catalysts used to assess if a partial deactivation could be observed. As can be seen in Figure 10, both TiO₂ and 5-NBC-TiO₂ show a marked deactivation, while 5-MBC-TiO₂ shows only a slight decrease in its photocatalytic efficiency.

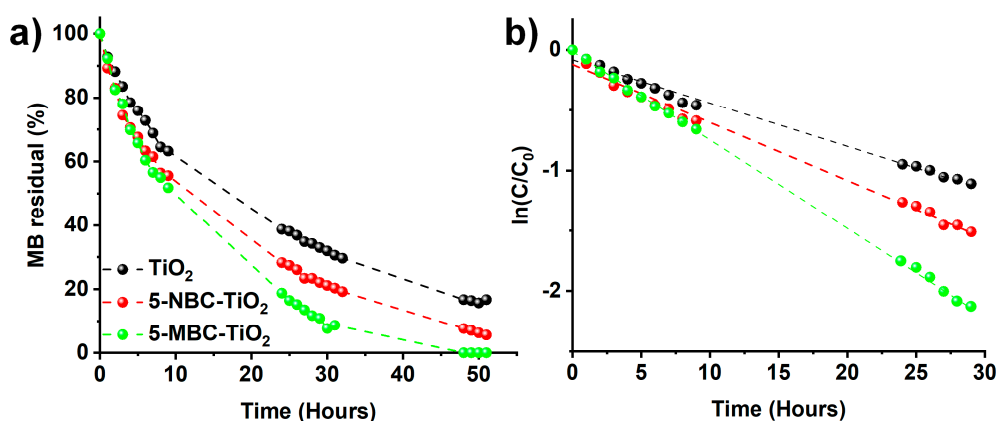


Figure 9. (a) Fifty-one-hour degradation tests performed on TiO₂ (black), 5-NBC-TiO₂ (red), and 5-MBC-TiO₂ (green). (b) Linearization by fitting with a first order kinetic model.

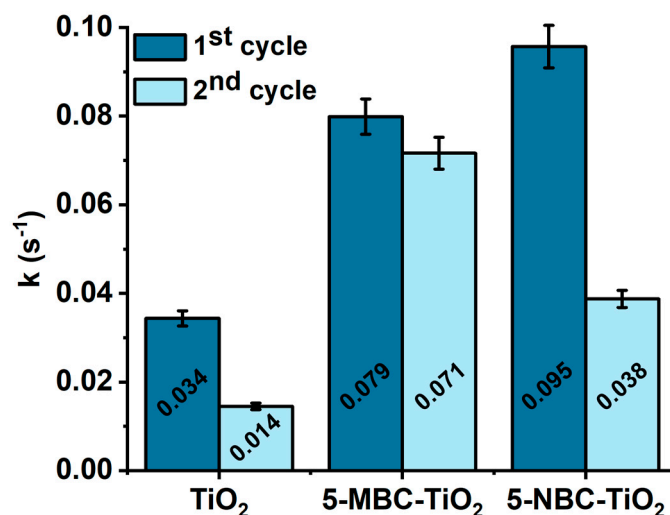


Figure 10. Kinetic constants for fresh and recycled photocatalysts: all values are calculated from the data collected within the first 3 h of reaction under mild conditions.

The reason behind the different behavior of the biochar materials can be ascribed to their different chemical composition; as reported in Section 2.1, the microalgae derived biochar presents a higher content in the oxygenated functional group and has a higher heteroatoms content altogether that results in a higher photocatalytic performance (likely due to a reduced recombination rate for electron–holes pairs). For the lignocellulosic-derived nanoparticles, it can instead be supposed that the enhanced photocatalyst activity is due to a higher MB adsorption compared to bare TiO₂; however, the lack of oxygenated functional groups and heteroatoms results in an overall less active material.

Concerning the kinetic model, data fit with a first order model (Figure 9b); thus, we reasonably assumed that the mechanism is comparable to what is reported in the literature: MB molecules are adsorbed on BC, and MB degradation proceeds via reaction with superoxide radicals produced from the reaction between water and photogenerated holes [36].

2.4. Comparison of MB Degradation Performances with Literature Data

The two best performing materials (5-MBC-TiO₂ and 5-NBC-TiO₂) and pristine TiO₂ NTs were tested under conditions closer to those most commonly reported in the literature for MB degradation, i.e., higher light power density and lower MB/catalyst ratios. These experiments were carried out to compare the performance of our materials against similar ones reported in the literature. It can be observed in Figure 11 that both MBC- and NBC-

derived materials could completely degrade methylene blue within 3 h and did not exhibit a remarkable difference in photocatalytic performances.

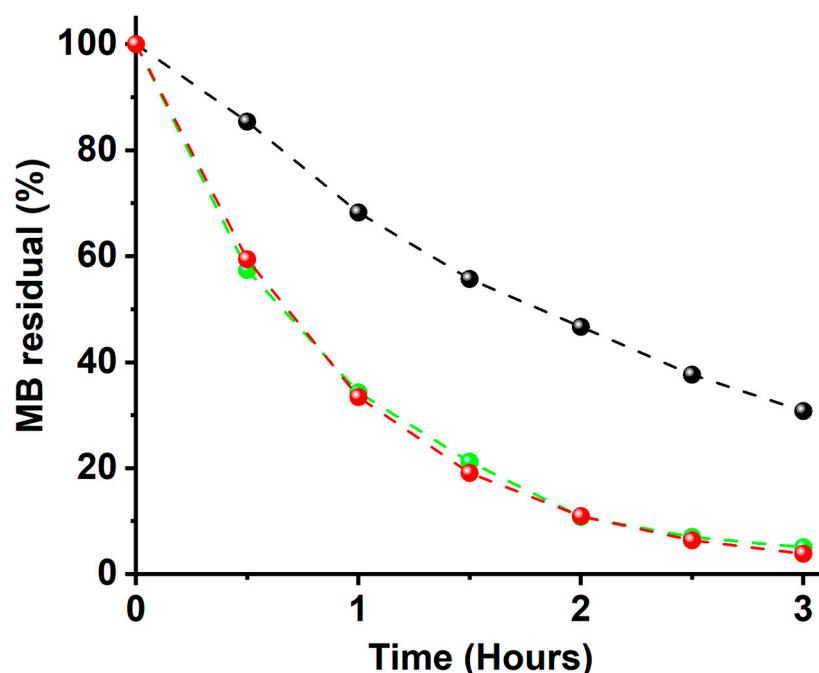


Figure 11. Kinetic curve obtained for MB photocatalytic degradation using bare TiO₂ (black line), 5-MBC-TiO₂ (green line), and 5-NBC-TiO₂ (red line) under boosted conditions.

A comparison of the performances of our materials against the BC-based ones reported in the literature is shown in Table 1. It should be underlined that, at present, only few articles report on MB degradation over BC-based photocatalysts. As a matter of fact, we did not find any data on BC-based planar photocatalysts, and thus only materials in powder form were considered for this comparison. In this respect, our systems represent the first examples of BC-decorated photocatalytic layers for this kind of application. Both microalgae- and nutshell-derived materials proposed in this work provide MB abatement rates comparable to or even higher than those reported for other BC-based photocatalysts. This is particularly interesting considering the much lower amount of co-catalyst present on our planar photocatalyst (in the range of micrograms) compared to that on reported materials. In any case, such an evaluation should be carefully considered owing to the quite different experimental conditions and photocatalyst form (i.e., planar platform vs. powder).

Table 1. Comparison of the photocatalytic performances towards MB degradation achieved in this work with those reported in the literature for other TiO₂-BC composite materials.

Photocatalyst	Biomass Feedstock	Experimental Conditions	% of MB Consumed in 2 h	Time for Complete MB Degradation	Reference
TiO ₂ nanotube arrays decorated with BC NPs	Microalgae (<i>Nannochloropsis</i> sp.)	(i) 10 mL of 10 mg/L MB; (ii) 100 mW/cm ² UV light (365 nm)	90%	3 h	This work
TiO ₂ nanotube arrays decorated with BC NPs	Nutshell	(i) 10 mL of 10 mg/L MB; (ii) 100 mW/cm ² UV light (365 nm)	90%	3 h	This work
BC impregnated with TiO ₂ (10% wt.)	Medium density fireboard	(i) 0.4 g/L of photocatalyst in 100 mg/L MB; (ii) 10 mW/m ² UV light (365 nm)	60%	n.a.	[59]
BC decorated with TiO ₂ NPs	Macroalgae	(i) 1 g/L of photocatalyst in 5 mg/L in MB solution (ii) 500 W visible light bulb	90%	3 h	[36]
BC-TiO ₂ hybrid material (10% wt.)	Plum stones	(i) 0.56 g/L of photocatalyst in 25 mg/L MB; (ii) Metal halide lamp (522.7 W/m ²)	≤50%	≥4 h	[60]
Powdered TiO ₂ nanotubes	n.a.	(i) 0.4 g/L of photocatalyst in 31 mg/L MB; (ii) 100 mW/cm ² UV light (365 nm)	85%	n.a.	[61]
Powdered Al-TiO ₂ nanotubes	n.a.	(i) 0.2 g/L of photocatalyst in 10 mg/L MB; (ii) 100 mW/cm ² UV light (365 nm)	90%	n.a.	[62]

With the aim of further highlighting the competitive performances of BC-TiO₂, different TiO₂-based systems used under similar testing conditions were also considered in the comparison of the photocatalytic performances. Even when compared with these less green systems, the photocatalytic activity exhibited by TiO₂ nanotube arrays decorated with BC NPs proposed in this work is comparable to or even higher than that reported for other TiO₂-based photocatalysts.

3. Materials and Methods

3.1. TiO₂ Nanotube Arrays Fabrication

Ti foils (99.945% purity, 0.03 mm thickness, William Gregor Ltd., London, UK) were degreased by sonicating in solvents of increasing polarity: acetone, isopropanol, ethanol, and ultrapure water. Each sonication step was conducted for 15 min and the samples were then dried under a N₂ stream. Subsequently, cleaned Ti foils (15 × 15 mm) were anodized at room temperature in an ethylene glycol solution containing ultrapure water (2% v/v, produced by a Sartorius Arium mini UV Lab Water System) and a fluoride concentration of 0.09 M (obtained by dissolving NH₄F, Merck, Kenilworth, NJ, USA). A two-electrode configuration was used for the anodization, where the Ti foil was the working electrode, and a graphite plate was the counter electrode. The anodization was performed by applying a potential of 40 V (for 60 min) using a DC power supply (Wanptek NPS1230W). The anodized samples were rinsed and soaked in ethanol for at least 30 min. The as-formed (amorphous) TiO₂ nanotubes were then annealed and crystallized at 450 °C for 1 h in air with a heating ramp of 5 °C/min.

3.2. Biochar Production

Biochar was produced by slow pyrolysis at low temperature (350 °C) of two different commercially available feedstocks: nutshells and the microalgae *Nannochloropsis* sp. Biomasses were treated as detailed in previous work [46]. Briefly, approximately 10 g of dried raw biomass feedstock were put in a quartz tubular furnace and heated at 350 °C with a ramp of 10 °C/min under N₂ stream (0.5 L/min). Isothermal conditions at 350 °C were kept for 1 h. The obtained biochar was pulverized using a Fritsch Pulverisette 0 agate ball mill. BC produced from nutshells and microalgae is labelled as NBC and MBC, respectively.

3.3. Fabrication of the Composite BC-TiO₂ Photocatalyst

The fabrication of the composite BC-TiO₂ photocatalysts is summarized in Figure 1. After pyrolysis, the bulk BC powder was dispersed in ultrapure water (10 g/L) and sonicated for 1 h at room temperature using a Branson 5800 ultrasonic bath; this process induces the partial breaking of BC to nanosized particles [47,63]. The so obtained BC suspension was then centrifugated at 3000 rpm for 30 min. The supernatant was collected and centrifuged again to further disperse the smaller particles. Finally, the suspension obtained by the second centrifugation was filtered using a 0.2 µm pore size membrane; the collected liquid, containing nanosized BC, was deposited by drop-casting (120 µL) onto the TiO₂ support. Then, the sample was dried under a laminar flow hood at room temperature for at least 6 h. The loading of BC was varied by performing multiple depositions (1, 3, 5, and 7 times): photocatalysts are accordingly labelled as *n*-MBC-TiO₂ and *n*-NBC-TiO₂, where “*n*” is the number of performed depositions.

3.4. Characterization of BC and BC-TiO₂

The complete characterization of the morphology and chemical composition of BC (as obtained by pyrolysis) is reported in detail in our previous work [46].

The morphology of TiO₂ NTs and BC-TiO₂ was studied using an XL30 Environmental Scanning Electron Microscope (ESEM FEG Philips) at 20kV in high vacuum condition. Transmission electron microscopy (TEM) and high-resolution TEM (HR-TEM) analysis were performed by a ZEISS LIBRA 200FE microscope. A small volume (20 µL) of the

suspension containing BC NPs was deposited onto a TEM grid to observe the morphology of as-formed NPs, i.e., before the deposition on the TiO₂ nanotubes substrate. The particle-size distribution of BC nanoparticles was determined by processing SEM images using the software ImageJ (National Institutes of Health (NIH), Bethesda, MD, USA). X-ray diffraction (XRD) data were recorded on a Siemens D5000 system using Cu-K α radiation, 40 kV, 40 mA, with a step of 0.03° (2 θ) and a scanning speed of 0.06°·s⁻¹. Diffuse reflectance UV-visible spectroscopy (DR-UV) measurement on solid samples and UV-vis analysis to determine the methylene blue concentration (in photocatalytic tests) were carried out using a Shimadzu UV-2600i spectrometer.

3.5. Photocatalytic Degradation of Methylene Blue

Methylene blue (MB) was selected as target molecule as this dye is widely studied and adopted as a pollutant model in the literature for the development of photocatalysts [27,43,64].

Photocatalytic tests under mild conditions were performed using a 250 mL quartz beaker placed on a magnetic stirrer to ensure the continuous mixing of the solution. Each experiment was performed using 100 mL of a 10 mg/L MB solution (obtained by dilution of a concentrated 1 g/L solution prepared by dissolving solid MB in ultrapure water) and an irradiation power of 40 mW/cm².

Boosted photocatalytic tests were performed using 10 mL of a 10 mg/L MB solution stirred in a quartz test tube with an irradiation power of 100 mW/cm².

An UV LED light source ($\lambda = 365$ nm, UVWave) with tunable power was used for both types of photocatalytic tests. Power density was measured by means of a thermal sensor (OptoSigma®).

MB concentration was monitored during the degradation tests by spectrophotometric means, recording absorbance values at 665 nm. A 30-min equilibration without light irradiation was performed before each photocatalytic test.

4. Conclusions

In this paper we demonstrated the feasibility of producing biochar-decorated TiO₂ photocatalysts by means of simple drop-casting. The composite BC-TiO₂ materials prepared in the present work proved to be more efficient than undecorated TiO₂ nanotubes towards the degradation of methylene blue under UV light irradiation; this evidence clearly indicates the ability of BC NPs to act as co-catalysts on the TiO₂ surface. The greatly enhanced sorption of organic molecules, together with improved charge carrier separation provided by BC NPs led to almost tripled photocatalytic performances.

It was observed that two types of biochar derived from markedly different biomasses (i.e., microalgae and nutshells) can promote MB decomposition to a similar extent, even if microalgae-derived BC is much less prone to deactivation than the nutshell-derived one. Further studies will be carried out to deeply understand the nature of the deactivation process and restore the original activity of the material.

Future perspectives might involve the optimization of reaction conditions to obtain the best photocatalytic performances and the application of biochar nanoparticle-decorated photocatalysts for the abatement of contaminants of emerging concern (e.g., pharmaceuticals such as acetaminophen).

Supplementary Materials: The following are available online at <https://www.mdpi.com/article/10.3390/catal11091048/s1>, Figure S1: SEM images of fresh biomass and bulk biochar, Figure S2: elemental composition of biochar, Figure S3: XRD patterns of MBC- and NBC-TiO₂, Figure S4: DR-UV spectra of MBC- and NBC-TiO₂.

Author Contributions: Conceptualization, D.S., D.M., and S.R.; methodology, M.P. and D.S.; investigation, M.P., D.S., G.B. and M.M.; formal analysis, M.P.; validation, M.P.; data curation, M.P., D.S. and G.B.; writing—original draft preparation, M.P. and D.S.; writing—review and editing, D.M., S.R.,

C.D. and M.A.; visualization, D.S. and G.B.; resources, C.D. and S.R.; supervision, C.D., D.M. and S.R. All authors have read and agreed to the published version of the manuscript.

Funding: This research received no external funding.

Conflicts of Interest: The authors declare no conflict of interest.

References

1. Liyanage, C.P.; Yamada, K. Impact of Population Growth on the Water Quality of Natural Water Bodies. *Sustainability* **2017**, *9*, 1405. [\[CrossRef\]](#)
2. Mills, A.; Davies, R.H.; Worsley, D. Water purification by semiconductor photocatalysis. *Chem. Soc. Rev.* **1993**, *22*, 417. [\[CrossRef\]](#)
3. Gopinath, K.P.; Madhav, N.V.; Krishnan, A.; Malolan, R.; Rangarajan, G. Present applications of titanium dioxide for the photocatalytic removal of pollutants from water: A review. *J. Environ. Manag.* **2020**, *270*, 110906. [\[CrossRef\]](#)
4. Zhao, Z.; An, H.; Lin, J.; Feng, M.; Murugadoss, V.; Ding, T.; Liu, H.; Shao, Q.; Mai, X.; Wang, N.; et al. Progress on the Photocatalytic Reduction Removal of Chromium Contamination. *Chem. Rec.* **2019**, *19*, 873–882. [\[CrossRef\]](#)
5. Spanu, D.; Dal Santo, V.; Malara, F.; Naldoni, A.; Turolla, A.; Antonelli, M.; Dossi, C.; Marelli, M.; Altomare, M.; Schmuki, P.; et al. Photoelectrocatalytic oxidation of As(III) over hematite photoanodes: A sensible indicator of the presence of highly reactive surface sites. *Electrochim. Acta* **2018**, *292*, 828–837. [\[CrossRef\]](#)
6. Spanu, D.; Bestetti, A.; Hildebrand, H.; Schmuki, P.; Altomare, M.; Recchia, S. Photocatalytic reduction and scavenging of Hg(II) over templated-dewetted Au on TiO₂ nanotubes. *Photochem. Photobiol. Sci.* **2019**, *18*, 1046–1055. [\[CrossRef\]](#)
7. Chatterjee, D.; Dasgupta, S. Visible light induced photocatalytic degradation of organic pollutants. *J. Photochem. Photobiol. C Photochem. Rev.* **2005**, *6*, 186–205. [\[CrossRef\]](#)
8. Gusain, R.; Gupta, K.; Joshi, P.; Khatri, O.P. Adsorptive removal and photocatalytic degradation of organic pollutants using metal oxides and their composites: A comprehensive review. *Adv. Colloid Interface Sci.* **2019**, *272*, 102009. [\[CrossRef\]](#) [\[PubMed\]](#)
9. Hashimoto, K.; Irie, H.; Fujishima, A. TiO₂ Photocatalysis: A Historical Overview and Future Prospects. *Jpn. J. Appl. Phys.* **2005**, *44*, 8269–8285. [\[CrossRef\]](#)
10. Nakata, K.; Fujishima, A. TiO₂ photocatalysis: Design and applications. *J. Photochem. Photobiol. C Photochem. Rev.* **2012**, *13*, 169–189. [\[CrossRef\]](#)
11. Al-Azri, Z.H.N.; Chen, W.-T.; Chan, A.; Jovic, V.; Ina, T.; Idriss, H.; Waterhouse, G.I.N. The roles of metal co-catalysts and reaction media in photocatalytic hydrogen production: Performance evaluation of M/TiO₂ photocatalysts (M = Pd, Pt, Au) in different alcohol–water mixtures. *J. Catal.* **2015**, *329*, 355–367. [\[CrossRef\]](#)
12. Spanu, D.; Recchia, S.; Mohajernia, S.; Schmuki, P.; Altomare, M. Site-selective Pt dewetting on WO₃-coated TiO₂ nanotube arrays: An electron transfer cascade-based H₂ evolution photocatalyst. *Appl. Catal. B Environ.* **2018**, *237*, 198–205. [\[CrossRef\]](#)
13. Meng, A.; Zhang, L.; Cheng, B.; Yu, J. Dual Cocatalysts in TiO₂ Photocatalysis. *Adv. Mater.* **2019**, *31*, 1807660. [\[CrossRef\]](#)
14. Spanu, D.; Minguzzi, A.; Recchia, S.; Shahvardanfard, F.; Tomanec, O.; Zboril, R.; Schmuki, P.; Ghigna, P.; Altomare, M. An Operando X-ray Absorption Spectroscopy Study of a NiCu–TiO₂ Photocatalyst for H₂ Evolution. *ACS Catal.* **2020**, *10*, 8293–8302. [\[CrossRef\]](#)
15. Iqbal, A.; Kafizas, A.; Sotelo-Vazquez, C.; Wilson, R.; Ling, M.; Taylor, A.; Blackman, C.; Bevan, K.; Parkin, I.; Quesada-Cabrera, R. Charge Transport Phenomena in Heterojunction Photocatalysts: The WO₃/TiO₂ System as an Archetypical Model. *ACS Appl. Mater. Interfaces* **2021**, *13*, 9781–9793. [\[CrossRef\]](#) [\[PubMed\]](#)
16. Mohamed, H.H.; Alomair, N.A.; Akhtar, S.; Youssef, T.E. Eco-friendly synthesized α -Fe₂O₃/TiO₂ heterojunction with enhanced visible light photocatalytic activity. *J. Photochem. Photobiol. A Chem.* **2019**, *382*, 111951. [\[CrossRef\]](#)
17. Altomare, M.; Nguyen, N.T.; Hejazi, S.; Schmuki, P. A Cocatalytic Electron-Transfer Cascade Site-Selectively Placed on TiO₂ Nanotubes Yields Enhanced Photocatalytic H₂ Evolution. *Adv. Funct. Mater.* **2018**, *28*, 1704259. [\[CrossRef\]](#)
18. Ji, L.; Spanu, D.; Denisov, N.; Recchia, S.; Schmuki, P.; Altomare, M. A Dewetted-Dealloyed Nanoporous Pt Co-Catalyst Formed on TiO₂ Nanotube Arrays Leads to Strongly Enhanced Photocatalytic H₂ Production. *Chem. An Asian J.* **2020**, *15*, 301–309. [\[CrossRef\]](#)
19. Spanu, D.; Recchia, S.; Mohajernia, S.; Tomanec, O.; Kment, Š.; Zboril, R.; Schmuki, P.; Altomare, M. Templated Dewetting–Alloying of NiCu Bilayers on TiO₂ Nanotubes Enables Efficient Noble-Metal-Free Photocatalytic H₂ Evolution. *ACS Catal.* **2018**, *8*, 5298–5305. [\[CrossRef\]](#)
20. Zielińska-Jurek, A. Progress, Challenge, and Perspective of Bimetallic TiO₂ -Based Photocatalysts. *J. Nanomater.* **2014**, *2014*, 208920. [\[CrossRef\]](#)
21. Woan, K.; Pyrgiotakis, G.; Sigmund, W. Photocatalytic Carbon-Nanotube-TiO₂ Composites. *Adv. Mater.* **2009**, *21*, 2233–2239. [\[CrossRef\]](#)
22. Yu, Y.; Yu, J.C.; Yu, J.-G.; Kwok, Y.-C.; Che, Y.-K.; Zhao, J.-C.; Ding, L.; Ge, W.-K.; Wong, P.-K. Enhancement of photocatalytic activity of mesoporous TiO₂ by using carbon nanotubes. *Appl. Catal. A Gen.* **2005**, *289*, 186–196. [\[CrossRef\]](#)
23. Minella, M.; Sordello, F.; Minero, C. Photocatalytic process in TiO₂/graphene hybrid materials. Evidence of charge separation by electron transfer from reduced graphene oxide to TiO₂. *Catal. Today* **2017**, *281*, 29–37. [\[CrossRef\]](#)

24. Chen, P.; Wang, F.; Chen, Z.-F.; Zhang, Q.; Su, Y.; Shen, L.; Yao, K.; Liu, Y.; Cai, Z.; Lv, W.; et al. Study on the photocatalytic mechanism and detoxicity of gemfibrozil by a sunlight-driven TiO₂/carbon dots photocatalyst: The significant roles of reactive oxygen species. *Appl. Catal. B Environ.* **2017**, *204*, 250–259. [[CrossRef](#)]
25. Wang, Q.; Huang, J.; Sun, H.; Zhang, K.Q.; Lai, Y. Uniform carbon dots@TiO₂ nanotube arrays with full spectrum wavelength light activation for efficient dye degradation and overall water splitting. *Nanoscale* **2017**, *9*, 16046–16058. [[CrossRef](#)] [[PubMed](#)]
26. Colmenares, J.C.; Varma, R.S.; Lisowski, P. Sustainable hybrid photocatalysts: Titania immobilized on carbon materials derived from renewable and biodegradable resources. *Green Chem.* **2016**, *18*, 5736–5750. [[CrossRef](#)]
27. Mian, M.M.; Liu, G. Recent progress in biochar-supported photocatalysts: Synthesis, role of biochar, and applications. *RSC Adv.* **2018**, *8*, 14237–14248. [[CrossRef](#)]
28. Cui, J.; Zhang, F.; Li, H.; Cui, J.; Ren, Y.; Yu, X. Recent progress in biochar-based photocatalysts for wastewater treatment: Synthesis, mechanisms, and applications. *Appl. Sci.* **2020**, *10*, 1019. [[CrossRef](#)]
29. Chen, Q.; Lin, G.; Meng, L.; Zhou, L.; Hu, L.; Nong, J.; Li, Y.; Wang, J.; Hu, K.; Yu, Q. Enhanced photoelectric performance of TiO₂ nanotubes sensitized with carbon dots derived from bagasse. *Chem. Phys. Lett.* **2020**, *749*, 137428. [[CrossRef](#)]
30. Guo, D.; Li, Y.; Cui, B.; Hu, M.; Luo, S.; Ji, B.; Liu, Y. Natural adsorption of methylene blue by waste fallen leaves of Magnoliaceae and its repeated thermal regeneration for reuse. *J. Clean. Prod.* **2020**, *267*, 121903. [[CrossRef](#)]
31. Ji, B.; Zhu, L.; Wang, S.; Liu, Y. Temperature-effect on the performance of non-aerated microalgal-bacterial granular sludge process in municipal wastewater treatment. *J. Environ. Manag.* **2021**, *282*, 111955. [[CrossRef](#)]
32. González-Castaño, M.; Morales, C.; Navarro de Miguel, J.C.; Boelte, J.H.; Klepel, O.; Flege, J.I.; Arellano-García, H. Are Ni/ and Ni₅Fe₁/biochar catalysts suitable for synthetic natural gas production? A comparison with γ -Al₂O₃ supported catalysts. *Green Energy Environ.* **2021**. [[CrossRef](#)]
33. Kant Bhatia, S.; Palai, A.K.; Kumar, A.; Kant Bhatia, R.; Kumar Patel, A.; Kumar Thakur, V.; Yang, Y.-H. Trends in renewable energy production employing biomass-based biochar. *Bioresour. Technol.* **2021**, *340*, 125644. [[CrossRef](#)]
34. Spanu, D.; Binda, G.; Dossi, C.; Monticelli, D. Biochar as an alternative sustainable platform for sensing applications: A review. *Microchem. J.* **2020**, *159*, 105506. [[CrossRef](#)]
35. Gibertini, E.; Liberale, F.; Dossi, C.; Binda, G.; Mattioli, B.; Bettinetti, R.; Maspero, A.; Fiore, M.; Ruffo, R.; Magagnin, L. Algae-derived hard carbon anodes for Na-ion batteries. *J. Appl. Electrochem.* **2021**. [[CrossRef](#)]
36. Fazal, T.; Razaq, A.; Javed, F.; Hafeez, A.; Rashid, N.; Amjad, U.S.; Ur Rehman, M.S.; Faisal, A.; Rehman, F. Integrating adsorption and photocatalysis: A cost effective strategy for textile wastewater treatment using hybrid biochar-TiO₂ composite. *J. Hazard. Mater.* **2020**, *390*, 121623. [[CrossRef](#)]
37. Zhao, L.; Cao, X.; Mašek, O.; Zimmerman, A. Heterogeneity of biochar properties as a function of feedstock sources and production temperatures. *J. Hazard. Mater.* **2013**, *256–257*, 1–9. [[CrossRef](#)]
38. Kloss, S.; Zehetner, F.; Dellantonio, A.; Hamid, R.; Ottner, F.; Liedtke, V.; Schwanninger, M.; Gerzabek, M.H.; Soja, G. Characterization of Slow Pyrolysis Biochars: Effects of Feedstocks and Pyrolysis Temperature on Biochar Properties. *J. Environ. Qual.* **2012**, *41*, 990–1000. [[CrossRef](#)] [[PubMed](#)]
39. Tomczyk, A.; Sokołowska, Z.; Boguta, P. Biochar physicochemical properties: Pyrolysis temperature and feedstock kind effects. *Rev. Environ. Sci. Bio/Technol.* **2020**, *19*, 191–215. [[CrossRef](#)]
40. Wang, W.; Zhang, J.; Chen, T.; Sun, J.; Ma, X.; Wang, Y.; Wang, J.; Xie, Z. Preparation of TiO₂-modified Biochar and its Characteristics of Photo-catalysis Degradation for Enrofloxacin. *Sci. Rep.* **2020**, *10*, 6588. [[CrossRef](#)]
41. Angin, D.; Altintig, E.; Köse, T.E. Influence of process parameters on the surface and chemical properties of activated carbon obtained from biochar by chemical activation. *Bioresour. Technol.* **2013**, *148*, 542–549. [[CrossRef](#)]
42. Ren, Q.; Wu, Z.; Hu, S.; He, L.; Su, S.; Wang, Y.; Jiang, L.; Xiang, J. Sulfur self-doped char with high specific capacitance derived from waste tire: Effects of pyrolysis temperature. *Sci. Total Environ.* **2020**, *741*, 140193. [[CrossRef](#)]
43. Zhu, Y.; Yi, B.; Yuan, Q.; Wu, Y.; Wang, M.; Yan, S. Removal of methylene blue from aqueous solution by cattle manure-derived low temperature biochar. *RSC Adv.* **2018**, *8*, 19917–19929. [[CrossRef](#)]
44. Xu, X.; Cao, X.; Zhao, L.; Wang, H.; Yu, H.; Gao, B. Removal of Cu, Zn, and Cd from aqueous solutions by the dairy manure-derived biochar. *Environ. Sci. Pollut. Res.* **2013**, *20*, 358–368. [[CrossRef](#)]
45. Fernandes, J.O.; Bernardino, C.A.R.; Mahler, C.F.; Santelli, R.E.; Braz, B.F.; Borges, R.C.; da Cunha Veloso, M.C.; Romeiro, G.A.; Cincotto, F.H. Biochar Generated from Agro-Industry Sugarcane Residue by Low Temperature Pyrolysis Utilized as an Adsorption Agent for the Removal of Thiamethoxam Pesticide in Wastewater. *Water Air Soil Pollut.* **2021**, *232*, 67. [[CrossRef](#)]
46. Binda, G.; Spanu, D.; Bettinetti, R.; Magagnin, L.; Pozzi, A.; Dossi, C. Comprehensive comparison of microalgae-derived biochar from different feedstocks: A prospective study for future environmental applications. *Algal Res.* **2020**, *52*, 102103. [[CrossRef](#)]
47. Plácido, J.; Bustamante-López, S.; Meissner, K.E.; Kelly, D.E.; Kelly, S.L. Microalgae biochar-derived carbon dots and their application in heavy metal sensing in aqueous systems. *Sci. Total Environ.* **2019**, *656*, 531–539. [[CrossRef](#)] [[PubMed](#)]
48. Liu, G.; Zheng, H.; Jiang, Z.; Zhao, J.; Wang, Z.; Pan, B.; Xing, B. Formation and Physicochemical Characteristics of Nano Biochar: Insight into Chemical and Colloidal Stability. *Environ. Sci. Technol.* **2018**, *52*, 10369–10379. [[CrossRef](#)]
49. Cha, G.; Schmuki, P.; Altomare, M. Anodic TiO₂ nanotube membranes: Site-selective Pt-activation and photocatalytic H₂ evolution. *Electrochim. Acta* **2017**, *258*, 302–310. [[CrossRef](#)]
50. Tansel, B.; Boglajenko, D. Characterization of aggregation and declustering tendency of hydrophobic fine particles in water. *Granul. Matter.* **2019**, *21*, 34. [[CrossRef](#)]

51. Albu, S.P.; Tsuchiya, H.; Fujimoto, S.; Schmuki, P. TiO₂ Nanotubes—Annealing Effects on Detailed Morphology and Structure. *Eur. J. Inorg. Chem.* **2010**, *2010*, 4351–4356. [[CrossRef](#)]
52. Altomare, M.; Pozzi, M.; Allieta, M.; Bettini, L.G.; Selli, E. H₂ and O₂ photocatalytic production on TiO₂ nanotube arrays: Effect of the anodization time on structural features and photoactivity. *Appl. Catal. B Environ.* **2013**, *136–137*, 81–88. [[CrossRef](#)]
53. Abdelmoula, M.; Sokoloff, J.; Lu, W.-T.; Close, T.; Menon, L.; Richter, C. Optical properties of titanium dioxide nanotube arrays. *J. Appl. Phys.* **2014**, *115*, 014306. [[CrossRef](#)]
54. Olgun, U.; Gülfen, M.; Üstel, F.; Arslan, H. Electro-Optics and Band Gap Energies of Nanosilver-Coated TiO₂ Nanotubes on Titanium Metal. *Acta Metall. Sin. Engl. Lett.* **2018**, *31*, 153–163. [[CrossRef](#)]
55. Li, J.; Wang, Y.; Wang, L. Structure and properties of nitrogen incorporated in TiO₂ nanotubes array. *Mater. Res. Express* **2014**, *1*, 025040. [[CrossRef](#)]
56. Helwig, A.; Müller, G.; Paul, S. Health monitoring of aviation hydraulic fluids using opto-chemical sensor technologies. *Chemosensors* **2020**, *8*, 131. [[CrossRef](#)]
57. Pang, Y.L.; Law, Z.X.; Lim, S.; Chan, Y.Y.; Shuit, S.H.; Chong, W.C.; Lai, C.W. Enhanced photocatalytic degradation of methyl orange by coconut shell-derived biochar composites under visible LED light irradiation. *Environ. Sci. Pollut. Res.* **2021**, *28*, 27457–27473. [[CrossRef](#)]
58. Xie, X.; Li, S.; Zhang, H.; Wang, Z.; Huang, H. Promoting charge separation of biochar-based Zn-TiO₂/pBC in the presence of ZnO for efficient sulfamethoxazole photodegradation under visible light irradiation. *Sci. Total Environ.* **2019**, *659*, 529–539. [[CrossRef](#)]
59. Silvestri, S.; Stefanello, N.; Sulkovski, A.A.; Foletto, E.L. Preparation of TiO₂ supported on MDF biochar for simultaneous removal of methylene blue by adsorption and photocatalysis. *J. Chem. Technol. Biotechnol.* **2020**, *95*, 2723–2729. [[CrossRef](#)]
60. Matos, J. Eco-Friendly Heterogeneous Photocatalysis on Biochar-Based Materials under Solar Irradiation. *Top. Catal.* **2016**, *59*, 394–402. [[CrossRef](#)]
61. Ciobanu, V.; Plesco, I. TiO₂ nanotubes for photocatalytic degradation of methylene blue. *J. Eng. Sci.* **2021**, *28*, 23–30. [[CrossRef](#)]
62. Song, Y.S.; Kim, Y.; Lee, H.; Lee, D.Y.; Lee, M.H.; Kim, B.Y. Photocatalytic Activity of Al-TiO₂ Nanomaterials for the Degradation of Methylene Blue Dye. *J. Korean Phys. Soc.* **2018**, *72*, 412–416. [[CrossRef](#)]
63. Meng, W.; Bai, X.; Wang, B.; Liu, Z.; Lu, S.; Yang, B. Biomass-Derived Carbon Dots and Their Applications. *Energy Environ. Mater.* **2019**, *2*, 172–192. [[CrossRef](#)]
64. Abdellah, M.H.; Nosier, S.A.; El-Shazly, A.H.; Mubarak, A.A. Photocatalytic decolorization of methylene blue using TiO₂/UV system enhanced by air sparging. *Alexandria Eng. J.* **2018**, *57*, 3727–3735. [[CrossRef](#)]